International Journal of Mechanical, Industrial and Aerospace Sciences
ISSN: 2517-9950
Vol:6, No:12, 2012

A Study on Prediction of Cavitation for Centrifugal Pump

Myung Jin Kim, Hyun Bae Jin, and Wui Jun Chung

***Abstract*—**In this study, to accurately predict cavitation of a centrifugal pump, numerical analysis was compared with experimental results modeled on a small industrial centrifugal pump. In this study, numerical analysis was compared with experimental results modeled on a small industrial centrifugal pump for reliable prediction on cavitation of a centrifugal pump. To improve validity of the numerical analysis, transient analysis was conducted on the calculated domain of full-type geometry, such as an experimental apparatus. The numerical analysis from the results was considered to be a reliable prediction of cavitaion.

***Keywords*—**Centrifugal Pump, Cavitation, NPSH, CFD.

I. Introduction

A CENTRIFUGAL pump is required to facilitate high performance and expend operation ranges with the development of industries in the variable field. The study focuses on variation of suction conditions relative to cavitation. Cavitation occurring in the inlet pipe was found to cause a decrease in performance because of a reduction or closure of flow passage and vibration. Also, cavitation generates noise by making cavitation extinct. If cavitation continues, erosion occurs at the wall of both the impeller and volute casing because of the impact of extinction. Therefore, to design the pump with high performance and expended suction conditions, a reliable prediction of cavitation is necessary.

Examining studies conducted on cavitation to date, predictions of cavitation and internal flow are investigated through numerical analysis [1-2], and the reliability of numerical analysis is validated through the experimental method [3-4]. Also, cavitation is predicted by using the acoustic emission and vibration envelope analysis [5-6].

In this study, to improve the accuracy on the prediction of cavitation occurring in the centrifugal pump through the numerical analysis, performance curve of experimental results for single-phase flow on a small industrial centrifugal pump compares with results of numerical analysis. On the basis of the results, the accuracy on the prediction of numerical analysis was improved by correcting cavitation coefficient for two-phase numerical analyses and this result was verified through the comparison with experimental results.

Myung Jin Kim is with the Mechanical Engineering Department, University of Ulsan, Ulsan, Republic of Korea (phone: 82-052-259-1614; e-mail: korykmj@ mail.ulsan.ac.kr).

Hyun Bae Jin is with the Mechanical Engineering Department, University of Ulsan, Ulsan, Republic of Korea (phone: 82-052-259-1614; e-mail: puhahazzang7@ mail.ulsan.ac.kr).

Wui Jun Chung is with the Mechanical Engineering Department, University of Ulsan, Ulsan, Republic of Korea (e-mail: wjchung@ mail.ulsan.ac.kr).

II. Experimental Apparatus and Method

A. Experimental Apparatus

Fig. 1 shows the layout of cavitation-experimental apparatus of the centrifugal pump and consists of three parts: a centrifugal pump, a vacuum tank, and a vacuum pump. A system consisting of the vacuum tank and the vacuum pump is the device that maintains vacuum levels at the inlet pressure of the centrifugal pump. The vacuum tank and the centrifugal pump are composed in a sealed cyclic type. The vacuum tank is designed with a capacity of 200L considering the cyclic flow of the pump. At the internal vacuum tank and the inlet of the vacuum pump, the ball tap valve and the pressure reducing valve are installed for stable water levels and vacuum levels, respectively. As for the water ring type, it is possible for the vacuum pump to vacuumize up to 17 torr (2.27 kPa). The specifications of the experimental centrifugal pump are shown in Table I.

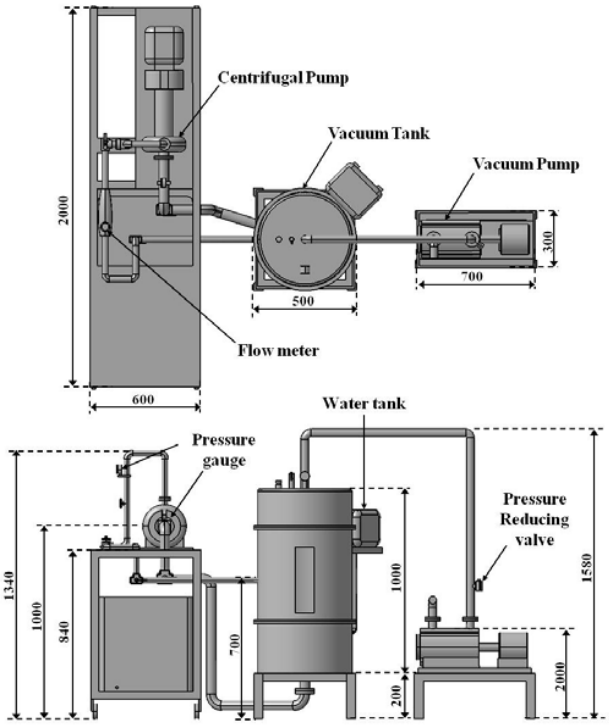

Fig. 1 Layout of experimental apparatus

TABLE I
SPECIFICATIONS OF THE CENTRIFUGAL PUMP

Number of blade	5
Range of flow coefficient (ϕ)	0 ~ 0.09
Range of head coefficient (ψ)	0.35 ~ 0.42
Diameter of impeller outlet (mm)	128
Rotational speed (rpm)	2400

B. Experimental Method

As mentioned in the introduction, first, a performance test for the centrifugal pump is conducted to show the validity of numerical analysis. The pump is fixed at 2400 RPM, and the flow is changed by using the flow control valve. A measured point of flow is divided into 16 points, and the reliability is increased by repeating the process five times at each measured point. Next, a cavitation test is conducted to gradually reduce the inlet pressure of the pump below the atmospheric pressure at a constant flow. The pressure of the pump inlet is controlled by changing the vacuum levels of the vacuum tank connected to the vacuum pump. Also, the average value of the test repeated five times is used to improve reliability. In the experimental test, water at 23 $^{\circ}C$ is used as the working fluid, and the temperature of the water was 27 $^{\circ}C$ when the experimental test ended. To make the initial condition identical, whenever the test starts the water is replaced.

III. NUMERICAL ANALYSIS

A. Model and Grid

The centrifugal pump used in this study is a FHF 32-125 from LOWARA, and the geometry for numerical analysis is generated by using a scanning device, COMET5 4M. Fig. 2 is the impeller and casing of geometry used in the numerical analysis. Many studies on only the impeller have been conducted because of limited computer capacity and analysis time. But, because of the asymmetry of the volute casing, an accurate analysis is impossible with these methods. Therefore, to accurately analyze for real phenomena, full-type geometry is required despite the amount of time spent. Fig. 3 shows the entire grid by using ANSYS ICEM CFD, with a computational domain consisting of the impeller, volute casing, inlet pipe and outlet pipe. Inlet pressure and outlet pressure are measured at 230mm from the inlet and 650mm from the outlet, respectively. Therefore, for clarity of boundary conditions, the same pipes used in the experiment apparatus are included in the computational domain.

The numbers for the grid are 2,800,000 and 1,200,000 at the impeller and volute casing, respectively, and is 1,000,000 at the inlet and outlet pipes. So, a grid of 5,000,000 is used. Also, for accuracy of numerical analysis, a prism mesh with eight layers is used at the tetra mesh wall, and the value of y+ is less than 1.

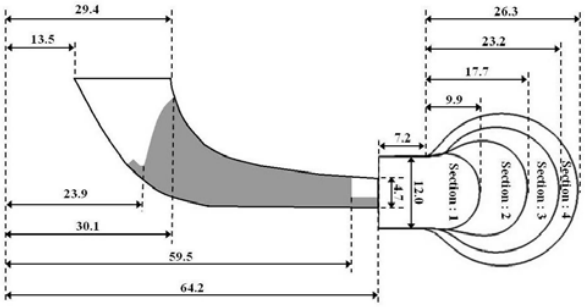

Fig. 2 Geometry and parameters of the centrifugal pump

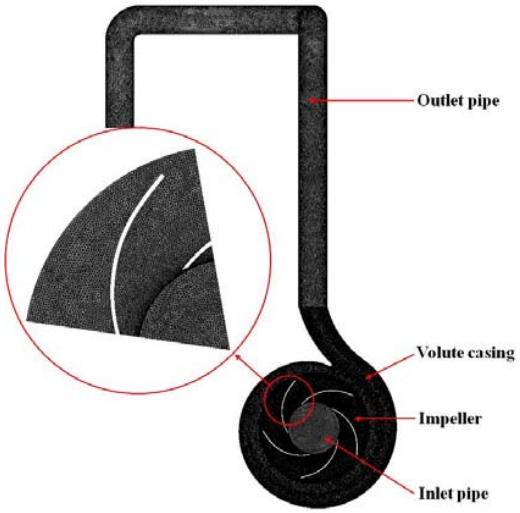

Fig. 3 Entire grid of the computational domain

B. Numerical Method

The numerical analysis is performed by using ANSYS CFX 13. The governing equation is a 3-dimension incompressible Reynolds-Averaged Navier-Stokes equation for a single-phase analysis and Eq. (1) representing the Rayleigh-Plesset model is used together with the above equation on cavitation analysis.

$$R_b \ddot{R}_b + \frac{3}{2}\dot{R}_b^2 + \frac{2\sigma_s}{\rho_f R_b} = \frac{P_v - P}{\rho_f} \quad (1)$$

In this equation, R_b, σ_s, ρ_f, P_v, and P refer to radius of bubble, surface tension coefficient, density of fluid, saturate vapor pressure, and pressure of fluid around vapor, respectively. The numerical analysis of the working fluid is water at 25 $^{\circ}C$ because the average temperature of the water used in the experiment is 25 $^{\circ}C$. The boundary conditions are total pressure and mass flow rate at the inlet and the outlet, respectively. The Transient Rotor Stator is applied at the interface between the impeller and the volute casing. The turbulence model is a sheer stress transport (SST) type, which gives an accurate result when analyzing turbo-machinery.

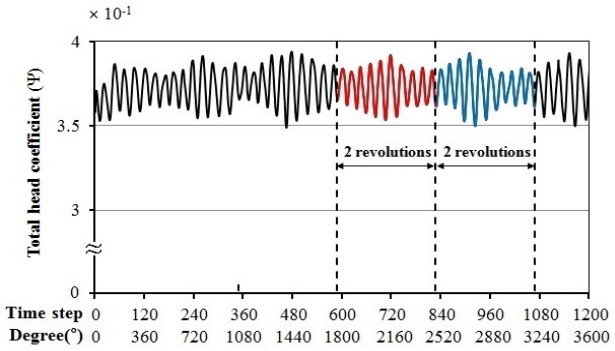

Fig. 4 The solution of transient analysis

Fig. 4 shows representative results of the numerical analysis. At this time, the time step is $2.857\times10^{-4}s$ (3°). In this figure, the maximum value and the minimum value appear at a periodicity of 36°. Such phenomena occur because of the effect of the tongue when the impeller blade rotates. Fig. 5 represents the end of the angle of the blade on the base of the throat. $\theta=34^{\circ}$ is the position most affected by the tongue, meaning that the tongue meets the end of the blade and $\theta=70^{\circ}$ is the position least affected by the tongue, which in turn means that the tongue is located in the middle of the impeller's passage. Therefore, transient analysis on the full-type geometry is required for an accurate analysis of the performance. In this study, after five revolutions, a similar periodicity of tendency is shown as for two revolutions. Based on this tendency, the average value of two revolutions provides the solution of transient analysis. In this study, all results of numerical analysis are gained through the above method.

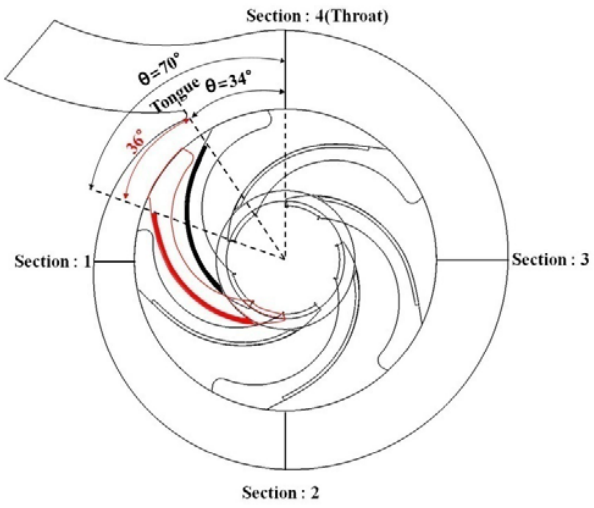

Fig. 5 Shape and position of impeller

IV. Result and Discussion

A. Pump Performance

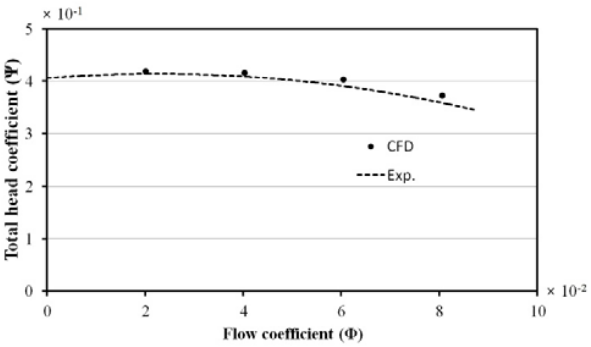

Fig. 6 Performance curves of experimental results and numerical analysis

Fig. 6 shows the performance of the pump compared with the experimental results and the numerical analysis in the single-phase analysis. In this figure, the x-axis and the y-axis represent flow coefficient(ϕ) and head coefficient(ψ), respectively, as in the following Eq. (2).

$$\phi=\frac{Q}{u_2\cdot A_2}\qquad \psi=\frac{g\cdot H_T}{u_2^{\,2}} \tag{2}$$

In these equations, Q, H_T, u_2, A_2, and g refer to flow, total head, peripheral velocity, area of impeller-outlet, and gravity, respectively. The experimental results of Fig. 5 represent the measured average value through curve-fitting at the range of flow. As the flow increases, a slight difference occurs, but the difference is not large and the shape of the curve shows the same tendency.

The errors of the experimental results and the numerical analysis on the head coefficient are shown in Table II. The numerical analysis is higher than the experimental results according to the increase of the flow coefficient. Such an error occurs because the numerical analysis did not apply to the leakage loss that occurs between the impeller and the casing and the mechanical loss that occurs between the bearing and the shaft. However, the result of the numerical analysis is quite acceptable because it presents an error of less than 3% over the entire flow.

TABLE II
Error of Performance Curves according to Flow Coefficient

Flow coef. $[\phi(10^{-2})]$	2.02	4.03	6.05	8.07
Exp. head coef. $[\psi_{Exp.}(10^{-1})]$	4.16	4.12	3.93	3.62
CFD. head coef. $[\psi_{CFD}(10^{-1})]$	4.19	4.17	4.03	3.73
Error (%) $[(\psi_{CFD}-\psi_{Exp.})/\psi_{Exp.}]$	0.7	1.2	2.5	3.0

B. Cavitation Performance

Fig. 7 shows total head according to variation of cavitation coefficient according for each flow coefficient. In this figure, Thoma's cavitation coefficient(σ) of the x-axis represents the suction capacity as in the following Eq. (3).

$$\sigma = \frac{NPSH}{H} \qquad NPSH = \frac{P_{in} - P_v}{\gamma} \tag{3}$$

In these equations, P_{in} and γ refer to total inlet pressure and specific gravity of water, respectively.

In the figure, the line on the horizontal x-axis refers to the constant head coefficient as for cavitation coefficient greater than 1, the average value of the points and the line perpendicular to the y- axis refer to the starting point of sudden reduction of the cavitation coefficient due to fully developed cavitation. The solid and dashed line in the figure refers to the numerical analysis and the experimental results, respectively. In the entire flow coefficient, the head coefficient maintains a constant value according to the decrease of the cavitation coefficient, and a sudden reduction of the head coefficient occurs due to cavitation after a small rise in the head. As such a phenomenon commonly appears both in numerical analysis and experimental results, those tendencies are similar, and the head coefficient of numerical analysis is slightly higher than the experimental head coefficient in the entire flow coefficient.

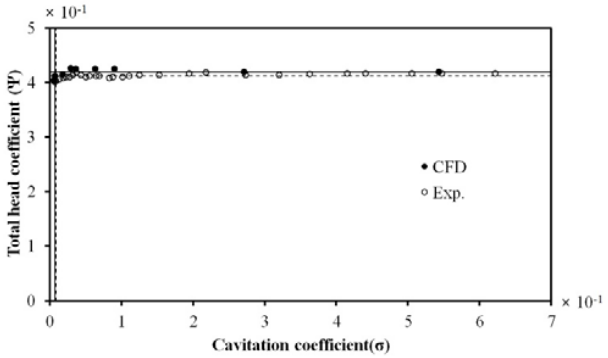

(a) ϕ =2.02(10^{-2})

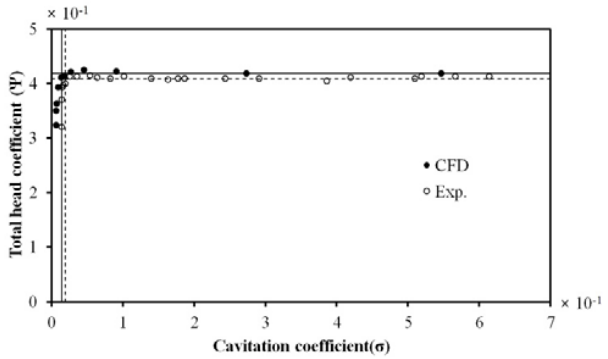

(b) ϕ =4.03(10^{-2})

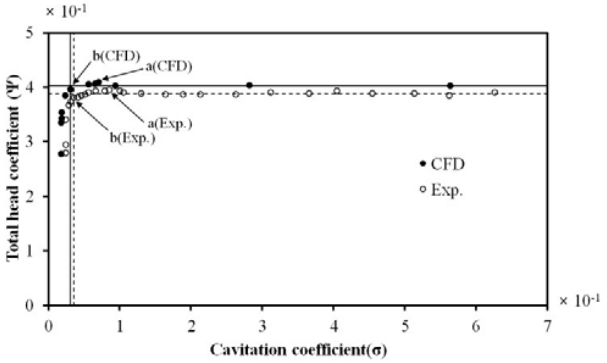

(c) ϕ =6.05(10^{-2})

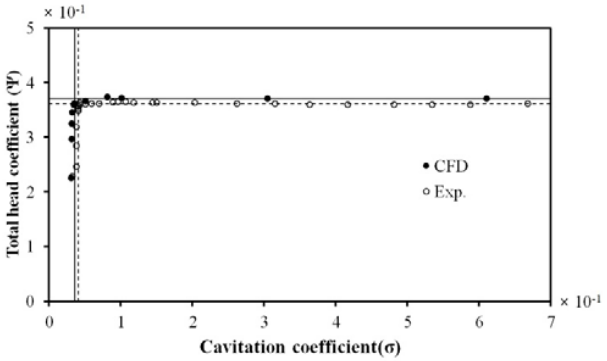

(d) ϕ =8.07(10^{-2})

Fig. 7 Comparison with the cavitation performance curve of experimental results and numerical analysis

Table III represents numerically the experimental results and numerical analysis presented in Fig. 7. In the table, the constant line refers to the line on the horizontal x-axis presented in Fig. 7. Also, a and b presented in ϕ =6.05(10^{-2}) of Fig. 7 refer to the point of a small rise in the head coefficient and the starting point of a sudden reduction. In the experimental results, a head rise on the basis of the head coefficient of the constant line until a is approximately 1.1% to 1.8%, averaging 1.5% and a head reduction on the basis a until b is approximately 3.5% to 3.6%, averaging 3.6%.On the other hand, numerical analysis present a head rise of approximately 0.8% to 1.7%, averaging 1.4% and a head reduction of approximately 3.2% to 3.3%, averaging 3.3%, respectively. In the entire flow coefficient, cavitation coefficient of a and b appear that the numerical analysis is smaller than the experimental results. As previously mentioned, these differences of results occur because the numerical analysis did not pay regard to the leakage loss and mechanical loss.

TABLE III
EXPERIMENTAL RESULT AND NUMERICAL ANALYSIS ACCORDING TO FLOW COEFFICIENT

Flow coef. $[\phi(10^{-2})]$	2.02	4.03	6.05	8.07
Exp. Head coef. of constant line $[\psi_l(10^{-1})]$	4.12	4.08	3.88	3.62
Exp. Cavitation coef. of a $[\sigma_a(10^{-2})]$	3.68	5.42	8.57	9.68
Exp. Head coef. of a $[\psi_a(10^{-1})]$	4.18	4.14	3.95	3.66
Exp. Cavitation coef. of b $[\sigma_b(10^{-2})]$	0.90	1.82	3.56	4.13
Exp. Head coef. of b $[\psi_b(10^{-1})]$	4.03	3.99	3.81	3.53
Exp. Rate of increase (%) $[(\psi_a-\psi_l)/\psi_l]$	1.5	1.5	1.8	1.1
Exp. Rate of decrease (%) $[(\psi_a-\psi_b)/\psi_a]$	3.6	3.6	3.5	3.6
CFD Head coef. of constant line $[\psi_l(10^{-1})]$	4.19	4.18	4.03	3.71
CFD Cavitation coef. of a $[\sigma_a(10^{-2})]$	2.90	4.55	7.05	8.14
CFD Head coef. of a $[\psi_a(10^{-1})]$	4.26	4.25	4.09	3.74
CFD Cavitation coef. of b $[\sigma_b(10^{-2})]$	0.72	1.37	3.10	3.56
CFD Head coef. of b $[\psi_b(10^{-1})]$	4.12	4.11	3.96	3.62
CFD Rate of increase (%) $[(\psi_a-\psi_l)/\psi_l]$	1.7	1.7	1.5	0.8
CFD Rate of decrease (%) $[(\psi_a-\psi_b)/\psi_a]$	3.3	3.3	3.2	3.2

To improve the accuracy of the prediction for numerical analysis on occurrence and establishment of cavitation, cavitation performance curve on the corrected numerical analysis by considering the difference of head of performance curve between experiment and numerical analysis and cavitation performance curve on the experimental results are represented in Fig. 8. In this figure, a correction of results of numerical analysis coincide with experimental results except for the value of ϕ =2.02(10^{-2}).

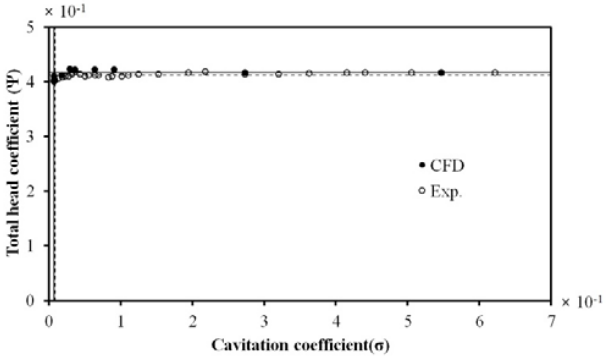

(a) ϕ =2.02(10^{-2})

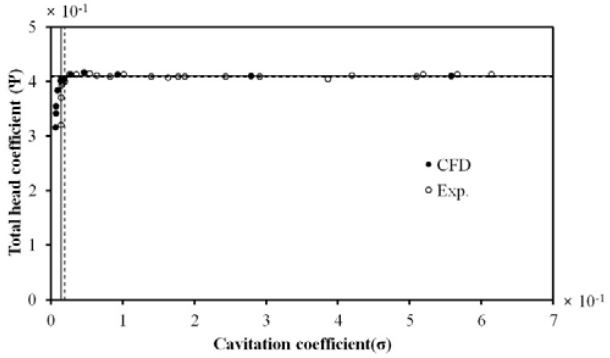

(b) ϕ =4.03(10^{-2})

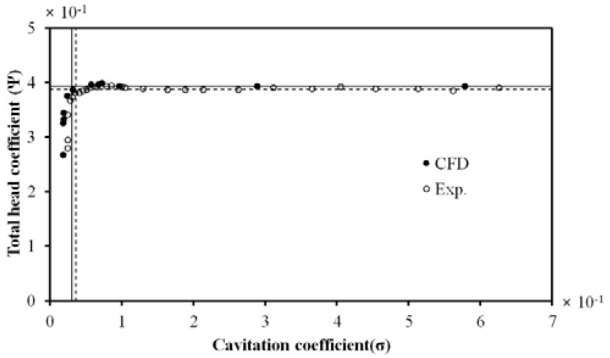

(c) ϕ =6.05(10^{-2})

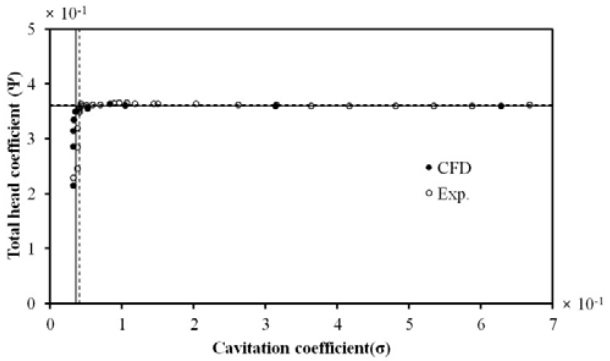

(d) ϕ =8.07(10^{-2})

Fig. 8 Comparison with cavitation performance curve of experimental results and corrected numerical analysis

Table IV represented numerically the corrected results of numerical analysis presented in Fig. 8 in the same way as Table III. In the table, a head rise on the basis of the head coefficient of the constant line until a is approximately 1.1% to 1.8%, averaging 1.5% and a head reduction on the basis a until b is approximately 3.5% to 3.6%, averaging 3.6%. Therefore, the corrected numerical values appear closer to the experimental values than the uncorrected numerical value. Also, reduced the difference between the experimental results can be found because cavitation coefficient of a and b in the entire flow increase slightly compared to the uncorrected results of numerical analysis.

TABLE IV
RESULT OF CORRECTION OF NUMERICAL ANALYSIS ACCORDING TO FLOW COEFFICIENT

Flow coef. $[\phi(10^{-2})]$	2.02	4.03	6.05	8.07
$CFD_{corr.}$ Head coef. of constant line $[\psi_l(10^{-1})]$	4.17	4.10	3.93	3.60
$CFD_{corr.}$ Cavitation coef. of a $[\sigma_a(10^{-2})]$	2.91	4.65	7.23	8.38
$CFD_{corr.}$ Head coef. of a $[\psi_a(10^{-1})]$	4.23	4.16	4.00	3.64
$CFD_{corr.}$ Cavitation coef. of b $[\sigma_b(10^{-2})]$	0.73	1.41	3.18	3.67
$CFD_{corr.}$ Head coef. of b $[\psi_b(10^{-1})]$	4.08	4.01	3.86	3.51
$CFD_{corr.}$ Rate of increase (%) $[(\psi_a-\psi_l)/\psi_l]$	1.4	1.5	1.8	1.1
$CFD_{corr.}$ Rate of decrease (%) $[(\psi_a-\psi_b)/\psi_a]$	3.5	3.6	3.5	3.6

Table V represents the differences between the numerical analysis and the correction of numerical analysis on the basis of the experimental results for a detecting the occurrence of cavitation and b presenting the establishment of cavitation, and the rate of improvement caused by the correction. The differences between the experimental results and the uncorrected results of numerical analysis are approximately 0.78, 0.87, 1.52, 1.54 at a and 0.18, 0.45, 0.46, 0.57 at b according to flow coefficient. After the correction, The differences are approximately 0.77, 0.77, 1.34, 1.3 at a and 0.17, 0.41, 0.38, 0.46 at b according to flow coefficient. Therefore, the accuracy of cavitaion coefficient of a and b is improved to 1.3%, 11.5%, 11.8%, 15.6%, averaging 10.1% and 5.6%, 8.9%, 17.4%, 19.3%, averaging 12.8% according to flow coefficient when the results of numerical analysis are corrected.

TABLE V
RATE OF IMPROVEMENT ACCORDING TO FLOW COEFFICIENT

Flow coef. $[\phi(10^{-2})]$	2.02	4.03	6.05	8.07
Difference of cavitation coef. of a $[Exp.-CFD]$ (10^{-2})	0.78	0.87	1.52	1.54
Difference of cavitation coef. of a $[Exp.-CFD_{corr.}]$ (10^{-2})	0.77	0.77	1.34	1.3
Rate of improvement (%) $[((Exp.-CFD)-(Exp.-CFD_{corr.}))/(Exp.-CFD)]$	1.3	11.5	11.8	15.6
Difference of cavitation coef. of b $[Exp.-CFD]$ (10^{-2})	0.18	0.45	0.46	0.57
Difference of cavitation coef. of b $[Exp.-CFD_{corr.}]$ (10^{-2})	0.17	0.41	0.38	0.46
Rate of improvement (%) $[((Exp.-CFD)-(Exp.-CFD_{corr.}))/(Exp.-CFD)]$	5.6	8.9	17.4	19.3

Eventually, these results are very similar to the experimental results when the computational domain is modeled on full-type geometry and the computational grid with a value of less than 1 is generated at least eight on the boundary layer of wall and numerical analysis is conducted through transient method. In addition, the accuracy is improved more than 10% by correcting the numerical analysis.

V. CONCLUSION

In this study, the following methods are presented to improve the accuracy of prediction on cavitaion occurrence of the centrifugal pump through the numerical analysis.

1) The computational domain is modeled on full-type geometry consisting of the impeller, volute casing, inlet pipe and outlet pipe.

2) The computational grid with a value of less than 1 is generated at least eight on the boundary layer of wall.

3) numerical analysis is conducted through transient method , considering the actual physical phenomena.

The numerical results obtained from such methods are similar to cavitation performance curve of experiment and the reliability of cavitation prediction for numerical analysis was validated. In addition, by using the difference between the experiment and numerical analysis on the correction of numerical analysis, averaging more than 10% of accuracy can be improved at cavitation coefficient detecting the occurrence of cavitation and cavitation coefficient presenting the establishment of cavitation.

REFERENCES

[1] X. Luo, Y. Zhang, J. Peng, H. Xu, and W. Yu, "Impeller inlet geometry effect on performance improvement for centrifugal pumps," *Journal of Mechanical Science and Technology*, vol.22, Oct. 2008.

[2] R. Fortes-Patella, O. Coutier-delgosha, J. perrin, and J. L. Reboud, "Numerical model to predict unsteady cavitation flow behavior in inducer blade cascade," *ASME Journal of Fluids Engineering*, vol. 129, Feb. 2007.

[3] B. Pouffary, R. Fortes-Patella, J. L. Rebound, and P. A. Lambert, "Numerical simulation of 3D cavitating Flows: Analysis of cavitation head drop in turbomachinery," *ASME Journal of Fluids Engineering*, vol. 130, Jun. 2008.

[4] D. Pierrat, L. Gros, A. Couzient, G. Pintrand, and Ph. Gyomlai, "On the leading edge cavitation in a helico-centrifugal pump : Experimental and numerical investigations," *3rd IAHR WG Meeting on Cavitation and Dynamic Problems in Hydraulic Machinery and Systems*, Oct. 2009.

[5] 2004, L. Alfayez, D. Mba, and G. Dyson "The application of acoustic emmisson for detecting incipient cavitation and the best efficiency point of a 60kW centrifugal pump: case studty," *ANDT & E international, vol.38*, 2003.

[6] C. Z. Tan, and M. S. Leong "An experimental study of cavitaion detection in a centrifugal pump using envelope analysis," *Journal of System Design and Dynamics*, Vol. 2, 2011.

[7] ANSYS-CFX Realease 13.0, *CFX-Solver Theory*.